Rashba-type spin accumulation near a void at a system edge

L. Y. Wang and C. S. Chu

Department of Electrophysics, National Chiao Tung University, Hsinchu 30010, Taiwan

(Received 1 February 2011; revised manuscript received 16 August 2011; published 30 September 2011)

We consider the spatial distribution of spin accumulation S_z near a void (edge void) located at a system edge. The edge void is semicircular in shape with a radius $R_0 \approx l_{so}$, the spin-relaxation length, and it is formed out of a Rashba-type two-dimensional electron system in the diffusive regime. The nonuniform driving field provides the essential condition, and diffusive contributions to the spin currents from spin polarizations provide the primary impetus for the spin accumulation. The edge void reveals an underlying asymmetry of the bulk-void counterpart, namely, a finite bulklike spin flow at the system edge. This bulklike spin flow gives rise to spin accumulation when open boundary occurs. The bulklike spin flow is found to exhibit a similar spatial profile as that of S_z at the system edge. This bulklike spin flow is expected to be a primary impetus for local spin injection at the sample edge near the edge void when a local protrusion occurs. Spin orientation of the bulklike spin flow varies with the locations on the edge-void boundary.

DOI: 10.1103/PhysRevB.84.125327 PACS number(s): 72.25.Dc, 71.70.Ej, 73.40.Lq

I. INTRODUCTION

All-electrical generations and manipulations of spin polarization are the main goals of semiconductor spintronics. Rashba spin-orbit interaction[1] (RSOI) has been the key knob for achieving this goal due to its gate-tuning capability.[2–4] However, in the diffusive regime ($l_{so} \gg l_e$), the RSOI's contribution to the edge-spin accumulation S_z is completely quenched due to the linear-k dependence of the SOI.[5–9] The edge-spin accumulation is an essential feature of spin Hall effect (SHE),[10–27] and k, l_{so}, and l_e are, respectively, the electron momentum, spin-relaxation length, and mean-free path. Although RSOI contributes to SHE in the mesoscopic ballistic regime[28,29] ($l_{so} < l_e$ and the system dimension $L < l_\phi$, the phase coherent length), it remains important to seek for ways to restore the RSOI contribution to edge-spin accumulation (or SHE) in the diffusive regime. Furthermore, the edge-spin accumulation, if current induced, could lead to spin injection into a region where the driving field is absent,[30] even though great care must be exercised when the RSOI is changed across the injection boundary.[31]

Effects of RSOI on SHE in the diffusive regime have been obtained at two corners of an electrode-sample interface[7,32] and in its competing interplay with the cubic-k Dresselhaus SOI (DSOI).[33] However, the former has the spin accumulation restricted to within a l_{so} region about the interface corners, whereas the latter has the RSOI restricted to suppressing the spin accumulations due to the cubic-k DSOI.[21,22] Seeking for more flexible ways of RSOI's contribution has prompted a recent study on a nonuniform field SHE.[34] A void in the bulk of a Rashba-type two-dimensional electron system (2DES) and its surrounding nonuniform driving field were found to generate a spin accumulation S_z.[34] The underlying physical process is different from the conventional one. While the conventional one is associated with a finite out-of-plane spin current (SC) I_ν^z, the key process in Ref. 25 is associated with an in-plane SC I_ν^μ, and with its vanishing at the edge-void boundary. Here, $\mu,\nu \in \{x,y\}$, and the superscript (subscript) denotes spin (flow) direction.

Spin accumulation at a system edge, however, is even more interesting in its own right,[26,27] and also in its possible connection with spin injection.[30,31,35] It is legitimate then to consider the spin accumulation near a void (edge void, see Fig. 1) at a system edge to get a clear physical understanding of the physical processes that contribute to the phenomenon, and to make connection with spin injection. In this work, we find out that the edge void (EV) reveals an underlying asymmetry, namely, a bulklike spin flow (spin-current source in the next section) at the system edge. This asymmetry feature does not produce spin density S_z in a bulk void along the longitudinal symmetry axis ($y = 0$),[34] but it is the sole source for the S_z at the sample edge in the case of an EV. Furthermore, we show that the spatial profile of the bulklike spin flow is quite similar to that of S_z at the system edge. As the bulklike spin flow provides a primary impetus for S_z when open boundary occurs, it will provide a primary impetus for spin injection when an elongated protrusion occurs at the sample edge near the edge void. The edge-spin-accumulation profile will thus provide us a guide for the favorable sites for spin injection. Detailed investigation of the specific spin retrieval scheme will be carried out in future study.

A physical picture for the spin-accumulation processes is presented below, and it starts from the finding in Ref. 25 that the nonuniform driving field $\boldsymbol{E}(\boldsymbol{\rho})$ gives rise to an Edelstein-type spin polarization[34]

$$\boldsymbol{S}_\parallel^{\mathrm{Ed}} = -N_0 \alpha \tau e/\hbar \; \hat{z} \times \boldsymbol{E}(\boldsymbol{\rho}), \tag{1}$$

for which spin is in plane and spatial variation at position $\boldsymbol{\rho}$ is from the driving field. Here, N_0, α, τ, and e are the energy density per spin, RSOI coupling constant, mean-free time, and charge magnitude, respectively. Already, $\boldsymbol{S}_\parallel^{\mathrm{Ed}}$ satisfies the spin-diffusion equation, but the boundary condition for the SC has not. The SC $I_n^i(\boldsymbol{S}, J_n^E)$ contains terms related to the spin polarization $\boldsymbol{S}$ and to the direct field-driving term J_n^E, and is given by[22,34,36]

$$\begin{aligned} I_n^\nu &= -2D\nabla_n S_\nu - R^{\nu z \nu} S_z \; (\hat{\nu}\cdot\hat{n}), \\ I_n^z &= -2D\nabla_n S_z - \sum_{\nu=x,y} R^{z\nu\nu} S_\nu \; (\hat{\nu}\cdot\hat{n}) + J_n^E, \end{aligned} \tag{2}$$

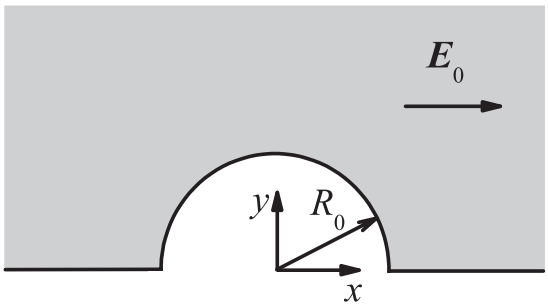

FIG. 1. An edge void of radius R_0 is positioned at a system edge. Asymptotic driving field is $\boldsymbol{E}_0$ and the origin of the coordinate coincides with the void center.

where the gradient terms correspond to diffusive contributions with D the diffusion constant, the $R^{\nu lm}$ denotes the precession of S_l into S_ν when the flow is along $\hat{m}$, and J_n^E corresponds to the direct effect of the driving field. Setting $\boldsymbol{S} = \boldsymbol{S}_\parallel^{\rm Ed}$ leads to zero I_n^z but nonzero I_n^ν. That the former SC is zero reflects the quenching of the conventional RSOI's contribution to SHE, but the nonzero value for the latter SC shows that diffusive contributions from in-plane spin polarization provide the primary impetus for the SHE. A nonuniform driving field opens up this unconventional contribution of RSOI to SHE. The condition $I_n^{\nu,z} = 0$ at the EV boundary ($\hat{n}$ normal to the boundary) generates an additional $\Delta\boldsymbol{S}$ including, most importantly, a nonzero spin accumulation $\Delta\boldsymbol{S}_z$, as is evident from the I_n^ν expression in Eq. (2). The conditions that the spin currents are zero at both the void boundary and the system edge, where the symmetries are incompatible, mandates a self-consistent procedure for the determination of the spin accumulation. To this end, we have devised a semianalytical approach, which provides us a transparent view of the physical processes involved.

The SC given by Eq. (2) has $D = v_F^2\tau/2$, where v_F is the Fermi velocity, and $R^{ilm} = 4\tau\sum_n \epsilon^{iln}\overline{h_k^n v_k^m}$, where ϵ^{iln} is the Levi-Civita symbol, $\boldsymbol{h_k}$ the effective RSOI field, and the overline denotes angular average over Fermi surface. The direct field-driving term in the SC is given by $J_n^E = \sum_\nu 4\tau^2\overline{v_k^n(\boldsymbol{h}_k \times \frac{\partial \boldsymbol{h}_k}{\partial k_l})_z} eN_0\nabla_l\varphi(\boldsymbol{r})$, where the nonuniform driving field $\boldsymbol{E} = -\nabla\varphi(\rho) = \sigma_0\boldsymbol{j}$ has the electric current density $\boldsymbol{j}$ satisfying the steady-state condition $\nabla\cdot\boldsymbol{j} = 0$ and the boundary condition $j_n = 0$ for $\hat{n}$ normal to the boundary. Here, σ_0 is the electric conductivity and $\boldsymbol{E} = E_0\hat{x} - E_0(R_0/\rho)^2(\cos 2\phi\hat{x} + \sin 2\phi\hat{y})$ outside the circular edge void, with ρ and ϕ being the coordinates originated from the EV center.

In this paper, we calculate the spin polarization $\boldsymbol{S}$ in the vicinity of the EV. Our result is in the form $\boldsymbol{S} = \boldsymbol{S}^B + \Delta\boldsymbol{S}^{\rm EV}$. The first term $\boldsymbol{S}^B = \boldsymbol{S}_\parallel^{\rm Ed} + \Delta\boldsymbol{S}^B$ is the spin polarization for a bulk circular void,[34] where $I_n^i(\boldsymbol{S}^B, J_n^E) = 0$ at the EV boundary. J_n^E's sole contribution to SC is in $i = z$ and is exactly canceled by that from $\boldsymbol{S}_\parallel^{\rm Ed}$. Along the seemingly symmetry axis ($\phi = 0,\pi$, or $y = 0$) of the bulk void, we find that the SCs $I_n^x(\boldsymbol{S}^B,0)$ and $I_n^z(\Delta\boldsymbol{S}^B,0)$ are nonzero for $\hat{n} = \hat{y}$. This hidden asymmetry in SC is revealed when the circular void is positioned at a system edge and is exhibited via its generation of an additional $\Delta\boldsymbol{S}^{\rm EV}$.

The calculation of $\Delta\boldsymbol{S}^{\rm EV}$ is carried out in a two-step procedure. The first step produces $\Delta\boldsymbol{S}^{E1}$, which, together with $\boldsymbol{S}^B$, has $I_n^i(\boldsymbol{S}^B + \Delta\boldsymbol{S}^{E1}, J_n^E) = 0$ at the sample edge ($y = 0$). This step is solved analytically and $\Delta\boldsymbol{S}^{E1}$ is found to have already incorporated an essential part of the spin accumulation at the system edge, especially at the corners junctioning the edge and the void boundary. The second, and final, step is to find $\Delta\boldsymbol{S}^{E2}$ such that, with $\Delta\boldsymbol{S}^{\rm EV} = \Delta\boldsymbol{S}^{E1} + \Delta\boldsymbol{S}^{E2}$, $\boldsymbol{S}$ satisfies the SC boundary conditions at both the void boundary and the system edge. All the $\Delta\boldsymbol{S}$'s above for each step are solutions to the spin-diffusion equation [Eq. (3)], but each has to satisfy a designated SC boundary condition and each is driven by a designated SC source term. Nonzero SC at the boundary or edge in a step of our calculation will be treated as a SC source term for the determination of $\Delta\boldsymbol{S}$ in the next step.

We note, in passing, that the SC is used for the establishment of a boundary condition for the spin-diffusion equation. A conventional form of the spin-current operator $J_l^i = (1/4)(V_l\sigma_i + \sigma_i V_l)$ is appropriate for hard wall boundary,[22,37,38] where the kinetic velocity $V_l = (1/i\hbar)[\hat{x}, H]$, and spin unit of $\hbar$ is implied. As the boundary condition is applied to a region much shorter in distance than $l_{\rm so}$ from the boundary, the effect of spin torque[39,40] should be of secondary importance here.

In the following, we present our model and theory for the nonuniform driving-field effects in the vicinity of an EV. Numerical results and discussions are presented in Sec. III. A conclusion is presented in Sec. IV.

II. MODEL AND THEORY

The spin-diffusion equation (SDE) for the case of nonuniform driving field has been derived in Ref. 25. For the case of RSOI, the Hamiltonian $H_{\rm so} = \boldsymbol{h}_k\cdot\boldsymbol{\sigma}$ has the effective SOI field $\boldsymbol{h}_k = -\alpha\hat{z}\times\boldsymbol{k}$, where $\boldsymbol{\sigma}$ denotes the Pauli matrices. The SDE is given by

$$\begin{aligned} D\nabla^2 S_\nu - \frac{\Gamma^{\nu\nu}}{\hbar^2}S_\nu + \frac{R^{\nu z\nu}}{\hbar}\nabla_\nu S_z - \frac{\boldsymbol{M}^{\nu 0}\cdot\nabla}{2\hbar^3}D_0^0 = 0, \\ D\nabla^2 S_z - \frac{\Gamma^{zz}}{\hbar^2}S_z - \frac{R^{zxx}}{\hbar}\nabla_x S_x - \frac{R^{zyy}}{\hbar}\nabla_y S_y = 0, \end{aligned} \tag{3}$$

where $\boldsymbol{S}$ is in units of $\hbar$.

The spin-charge coupling term is $-\boldsymbol{M}^{\nu 0}\nabla D_0^0$ where $\boldsymbol{M}^{\nu 0} = 4\tau^2\overline{h_k^3\frac{\partial n_k^\nu}{\partial \boldsymbol{k}}}$, and ∇D_0^0 becomes position dependent in a nonuniform driving field. Here, $D_0^0 = 2N_0 e\varphi(\boldsymbol{\rho})$, $\hat{n}_k = \boldsymbol{h}_k/h_k$, and $R^{z\nu\nu} = -R^{\nu z\nu} = -2h_F\, v_F\tau$ for RSOI. Furthermore, $\Gamma^{il} = 4\tau\overline{h_k^2(\delta^{il} - n_k^i n_k^l)}$ are the D'yakonov-Perel' (DP) spin-relaxation rates for which $\Gamma^{xx} = \Gamma^{yy} = \Gamma^{zz}/2 = 2h_F^2\tau$ in the RSOI case.[41] The boundary condition for the SDE, as mentioned above, is given by $I_n^i = 0$ for $\hat{n}$ normal to either the system edge or the EV boundary.

Our main goal is to solve for $\Delta\boldsymbol{S}^{\rm EV}$. Adding this term to $\boldsymbol{S}^B$, the spin polarization for a bulk circular void, will give us the total spin polarization $\boldsymbol{S}$. The expression for $\boldsymbol{S}^B$ has been obtained analytically,[34] but it is too lengthy and is not presented here. An essential part of $\Delta\boldsymbol{S}^{\rm EV}$, namely, $\Delta\boldsymbol{S}^{E1}$, is the spin accumulation at the system edge, and it can be captured by first applying our SC boundary condition to the edge at $y = 0$ and for $\hat{n} = \hat{y}$. The remaining part of $\Delta\boldsymbol{S}^{\rm EV}$, namely,

$\Delta \boldsymbol{S}^{E2}$, is obtained by imposing the SC boundary conditions at both the EV boundary and the sample edge. Thus, $\Delta \boldsymbol{S}^{\mathrm{EV}} = \sum_{j=1,2} \Delta \boldsymbol{S}^{Ej}$.

To address the SC boundary condition at the system edge, we start from the SDE for $\Delta \boldsymbol{S}^{Ej}$ ($j = 1,2$), which is obtained from Eq. (3), given by

$$\begin{aligned} \nabla^2 \Delta S_x^{Ej} - 4\Delta S_x^{Ej} + 4\nabla_x \Delta S_z^{Ej} &= 0, \\ \nabla^2 \Delta S_y^{Ej} - 4\Delta S_y^{Ej} + 4\nabla_y \Delta S_z^{Ej} &= 0, \\ \nabla^2 \Delta S_z^{Ej} - 8\Delta S_z^{Ej} - 4\nabla_x \Delta S_x^{Ej} - 4\nabla_y \Delta S_y^{Ej} &= 0. \end{aligned} \tag{4}$$

This equation has adopted a length unit $l_{\mathrm{so}} = \sqrt{D\tau_{\mathrm{so}}}$, where $\tau_{\mathrm{so}} = 2\hbar^2/(h_F^2\tau)$ and h_F is the RSOI field at the Fermi surface. A Fourier transform solution to this SDE with respect to x is facilitated by writing $\Delta \boldsymbol{S}^{Ej}$ in the form

$$\Delta S_i^{Ej} = \int dk \sum_{q=1,2,3} \eta_q^{(j)}(k)\, a_{iq}\, e^{ikx} e^{-\beta_q y}, \tag{5}$$

where index q denotes the qth mode of solution for the SDE and $e^{-\beta_q y}$ indicates that $\Delta \boldsymbol{S}^{Ej}$ is localized near the $y = 0$ edge. The eigenmodes, given by a_{iq}, depend on k, and the amplitude for each such mode is attributed to $\eta_q^{(j)}(k)$.

By substituting $\Delta \boldsymbol{S}^{Ej}$ into Eq. (4), we obtain

$$\begin{bmatrix} -k^2+\beta_q^2-4 & 0 & 4ik \\ 0 & -k^2+\beta_q^2-4 & -4\beta_q \\ -4ik & 4\beta_q & -k^2+\beta_q^2-8 \end{bmatrix} \begin{bmatrix} a_{xq} \\ a_{yq} \\ a_{zq} \end{bmatrix} = 0, \tag{6}$$

where $\beta_1 = \sqrt{k^2+4}$, $\beta_2 = \sqrt{k^2-2+2i\sqrt{7}}$, and $\beta_3 = \beta_2^*$. The eigenmodes are $(a_{i1}) = (1, g_1, 0)$, $(a_{i2}) = (g_2, g_3, 1)$, and $(a_{i3}) = (-g_2^*, g_3^*, 1)$ with $g_1 = ik/\sqrt{k^2+4}$, $g_2 = ik(3+i\sqrt{7})/8$, and $g_3 = ig_2\sqrt{k^2-2+2i\sqrt{7}}/k$. The fact that $\Delta \boldsymbol{S}^{Ej}$ are real requires $\eta_1^{(j)}$ to be pure imaginary and $\eta_2^{(j)}(k) = [\eta_3^{(j)}(-k)]^*$. The amplitudes $\eta_q^{(j)}(k)$ will be fixed by the SC boundary conditions.

The boundary condition $I_n^i(\boldsymbol{S}^B + \Delta \boldsymbol{S}^{E1}, J_n^E) = 0$ at $y = 0$, and $\hat{n} = \hat{y}$ is obtained from Eq. (2), given by

$$\begin{aligned} \left[-\frac{\partial}{\partial y}\left(\Delta S_x^{E1} + \Delta S_x^B\right) + 2\alpha\widetilde{E}\frac{R_0^2}{x^3}\right]_{y=0} &= 0, \\ \left[-\frac{\partial}{\partial y}\left(\Delta S_y^{E1} + \Delta S_y^B\right) - 2\left(\Delta S_z^{E1} + \Delta S_z^B\right)\right]_{y=0} &= 0, \\ \left[-\frac{\partial}{\partial y}\left(\Delta S_z^{E1} + \Delta S_z^B\right) + 2\left(\Delta S_y^{E1} + \Delta S_y^B\right)\right]_{y=0} &= 0, \end{aligned} \tag{7}$$

where $\widetilde{E} = eE_0N_0\tau/\hbar$, and the term involving $\widetilde{E}$ is due to $\boldsymbol{S}_{\parallel}^{\mathrm{Ed}}$. Note that, if the terms in Eq. (7) that involve $\Delta \boldsymbol{S}^B$ and $\widetilde{E}$ were to add up to zero for their respective equations, then $\Delta \boldsymbol{S}^{E1}$ would be obviously zero. However, the contrary turns out to be the case here. Therefore, by moving these $\Delta \boldsymbol{S}^B$ and $\widetilde{E}$ terms to the right-hand side of Eq. (7), they become the SC sources $f_i^{(1)}$ for the $\Delta \boldsymbol{S}^{E1}$ generation, as is given by

$$\begin{aligned} \left[-\frac{\partial}{\partial y}\Delta S_x^{E1}\right]_{y=0} &= f_x^{(1)}, \\ \left[-\frac{\partial}{\partial y}\Delta S_y^{E1} - 2\Delta S_z^{E1}\right]_{y=0} &= f_y^{(1)}, \\ \left[-\frac{\partial}{\partial y}\Delta S_z^{E1} + 2\Delta S_y^{E1}\right]_{y=0} &= f_z^{(1)}, \end{aligned} \tag{8}$$

where $f_i^{(1)} = -I_y^i(\boldsymbol{S}_{\parallel}^{\mathrm{Ed}} + \Delta \boldsymbol{S}^B, J^E)|_{y=0}$ for $|x| \geqslant R_0$ and $f_i^{(1)} = 0$ for $|x| < R_0$. Analytical forms of $f_i^{(1)}$ are obtained to be

$$\begin{aligned} f_x^{(1)}(x) &= \frac{4\pi}{x}\{-X_2 + 2\,\mathrm{Im}[gZ_2]\} - 2\alpha\widetilde{E}\frac{R_0^2}{x^3}, \\ f_y^{(1)}(x) &= 0, \\ f_z^{(1)}(x) &= -\frac{4\pi}{|x|}\mathrm{Im}[Z_1] + 4\pi\{X_0 + 2\,\mathrm{Im}[gZ_0]\} \\ &\quad + 4\pi\{-X_2 + 2\,\mathrm{Im}[gZ_2]\}, \end{aligned} \tag{9}$$

where $g = \gamma_2/(\gamma_2^2+4)$, $X_m = it_x H_m^{(1)}(\gamma_1|x|)$, and $Z_m = t_z H_m^{(1)}(\gamma_2|x|)$. Here, $H_m^{(1)}(z)$ denotes the Hankel function of the first kind, and the constants $\gamma_1 = 2i$ and $\gamma_2 = \sqrt{2+2i\sqrt{7}}$. [34] Explicit expressions for t_x and t_z are not shown here, but they were defined for the expression of $\boldsymbol{S}^B$ in a bulk circular void.[34] Specifically, both t_x and t_z depend linearly on α, the RSOI coupling constant.

It is worth mentioning that $f_i^{(1)}$ can also be interpreted as a bulklike spin flow at the system edge, which gives rise to the edge-spin accumulation, as is evident in Eq. (8). Furthermore, $f_i^{(1)} \neq 0$ reflects an unexpected asymmetry. The symmetric structure of a bulk circular void seems to suggest that all currents, including charge and spin, flowing normally to the symmetry axis ($\phi = 0, \pi$) must be zero. This is indeed the case for the charge current, but is otherwise for the spin current. The reason is related to the fact that $\boldsymbol{S}_x^B$ and $\boldsymbol{S}_z^B$ are odd in y, while that for $\boldsymbol{S}_y^B$ is even.[34] As a consequence, according to Eq. (2), there are diffusive contributions to $f_x^{(1)}$ and $f_z^{(1)}$ but not to $f_y^{(1)}$. Furthermore, there is an additional contribution to $f_z^{(1)}$ through the spin precession of $\boldsymbol{S}_y^B$. Thus, we have nonzero $f_i^{(1)}$ except for $i = y$, as is shown in Fig. 2(a).

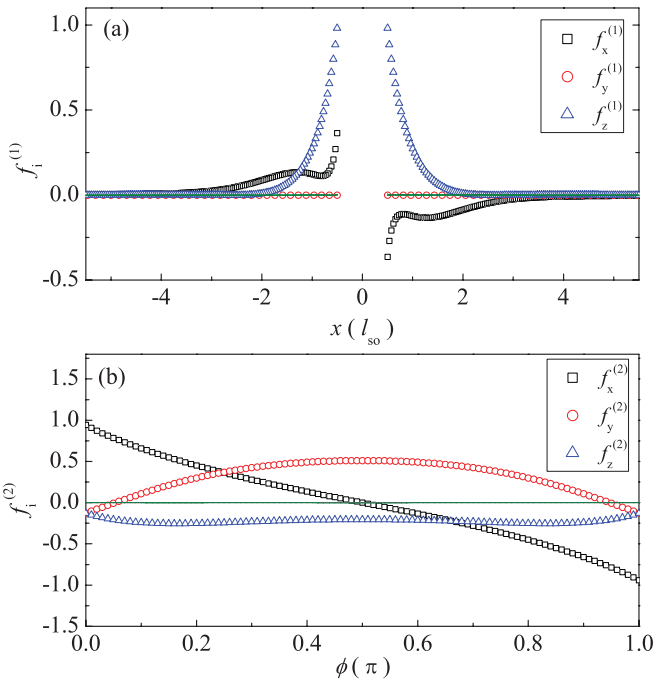

FIG. 2. (Color online) Spin-current source terms $f_i^{(j)}$ for $j = 1,2$ are plotted, respectively, in (a), (b), and with abscissas x and ϕ. In (a), empty symbols denote $\boldsymbol{f}_i^{(1)}$, and solid lines denote SC I_y^i at $y = 0$ when $\Delta \boldsymbol{S}^{E1}$ is included. In (b), open symbols denote $\boldsymbol{f}_i^{(2)}$, and solid lines denote SC I_n^i for $\hat{n} = \hat{\rho}$ and at $\rho = R_0$ when the total $\boldsymbol{S}$ is used.

The amplitudes $\eta_q^{(1)}(k)$ for the q modes are determined by Fourier transforming Eq. (8), via the integral $\frac{1}{2\pi}\int dx\, e^{-i\kappa x}$, to obtain

$$\begin{bmatrix} \beta_1 & \beta_2 g_2 & -\beta_3 g_2^* \\ \beta_1 g_1 & \beta_2 g_3 - 2 & \beta_3 g_3^* - 2 \\ 2g_1 & \beta_2 + 2g_3 & \beta_3 + 2g_3^* \end{bmatrix} \begin{bmatrix} \eta_1^{(1)} \\ \eta_2^{(1)} \\ \eta_3^{(1)} \end{bmatrix} = \begin{bmatrix} \tilde{f}_x^{(1)} \\ 0 \\ \tilde{f}_z^{(1)} \end{bmatrix}, \quad (10)$$

and from it, the $\eta_q^{(1)}(k)$. Here, $\tilde{f}_i^{(1)}(\kappa)$ is the Fourier transform of $f_i^{(1)}$.

The amplitudes $\eta_q^{(2)}(k)$ for $\Delta \boldsymbol{S}^{E2}$ can be calculated similarly. However, we need to address both the SC boundary conditions at the EV boundary and the system edge. The construction of $\Delta \boldsymbol{S}^{E1}$ has removed any further need of introducing the SC source at the system edge. Yet, additional spin polarization is generated because the SC from $\Delta \boldsymbol{S}^{E1}$ does not satisfy the boundary condition at the EV boundary. In effect, this gives rise to a SC source at the EV boundary that, in turn, generates $\Delta \boldsymbol{S}^{E2}$. In this work, we find out that it is convenient to replace the SC sources $f_i^{(2)}$ at the EV boundary by an auxiliary SC source $f_i^{\rm aux}$ at $y = 0$, but located outside the system edge, for $|x| < R_0$. This approach is in line with the concept of introducing image charges for the electrostatic problem where the image charges that help satisfy the boundary condition for the electrostatic potential must locate outside the region of interest. Taking into account the parity of $\boldsymbol{S}^B$ with respect to x, the auxiliary SC sources $f_i^{\rm aux}(|x| < R_0)$ are written in the form

$$\begin{aligned} f_x^{\rm aux}(x) &= f_{x0}^{\rm aux} + \sum_{n=1,2,\ldots} A_{x,n} \sin\left(\frac{n\pi x}{R_0}\right), \\ f_y^{\rm aux}(x) &= f_{y0}^{\rm aux} + \sum_{n=1,2,\ldots} A_{y,n} \cos\left(\frac{(2n-1)\pi x}{2R_0}\right), \\ f_z^{\rm aux}(x) &= f_{z0}^{\rm aux} + \sum_{n=1,2,\ldots} A_{z,n} \cos\left(\frac{(2n-1)\pi x}{2R_0}\right), \end{aligned} \quad (11)$$

where $f_{i0}^{\rm aux} = [f_x^{(1)}(R_0)\,x/R_0, 0, f_z^{(1)}(R_0)]$ is to make sure that $f_i^{\rm aux}$ connects to $f_i^{(1)}$ continuously to avoid the Gibbs phenomenon in the Fourier transformation. With the Fourier transformed auxiliary SC sources $\tilde{f}_i^{\rm aux}$ substituted into the right-hand side of Eq. (10), the column vector on the left-hand side of the equation becomes $\eta_i^{(2)}$. Thus, $\eta_i^{(2)}$ and $\Delta \boldsymbol{S}^{E2}$ are expressed in terms of $A_{j,n}$. These $A_{j,n}$ coefficients will then be fixed by the SC boundary condition at the EV boundary $I_n^i(\rho = R_0) = 0$, which is obtained from Eq. (2), given by

$$\begin{aligned} \left[-\frac{\partial}{\partial\rho}\Delta S_x^{\rm EV} - 2\cos\phi\,\Delta S_z^{\rm EV}\right]_{\rho=R_0} &= 0, \\ \left[-\frac{\partial}{\partial\rho}\Delta S_y^{\rm EV} - 2\sin\phi\,\Delta S_z^{\rm EV}\right]_{\rho=R_0} &= 0, \\ \left[-\frac{\partial}{\partial\rho}\Delta S_z^{\rm EV} + 2\cos\phi\,\Delta S_x^{\rm EV} + 2\sin\phi\,\Delta S_y^{\rm EV}\right]_{\rho=R_0} &= 0, \end{aligned} \quad (12)$$

where $\phi \in (0,\pi)$. Similar to Eq. (10), the contributions from $\Delta \boldsymbol{S}^{E1}$ in Eq. (12) will become the SC source $f_i^{(2)}$ when it is moved to the right-hand side of the equation. Solving the equation by direct discretization leads us to the total spin polarization $\boldsymbol{S} = \boldsymbol{S}^B + \Delta \boldsymbol{S}^{\rm EV}$.

III. NUMERICAL RESULTS

Numerical examples presented in this section are organized as follows. Figure 2 illustrates the effectiveness of our approach. Figures 3 and 4 present our main results that, respectively, spin accumulation $\boldsymbol{S}_z$ does occur near an EV due to RSOI and the S_z exhibits similar spatial profile as the bulklike spin flow at the system edge. The spin accumulation $\boldsymbol{S}_z$ for voids of large ($R_0 \gg l_{\rm so}$) and small ($R_0 \ll l_{\rm so}$) radii are shown in Figs. 5 and 6. Finally, Fig. 7 presents the distribution of the spin accumulation as probed by a scanning optical beam.

We have assumed material parameters that are consistent with GaAs. Specifically, the effective mass $m^* = 0.067m_0$, with m_0 the free-electron mass, electron density $n_e = 1 \times 10^{12}$ cm^{-2}, electron mean-free path $l_e = 0.43$ μm, the Rashba coupling constant $\alpha = 0.3 \times 10^{-12}$ eV m,[2,42] and the spin-relaxation length $l_{\rm so} = 3.76$ μm. Furthermore, the driving field $E_0 = 40$ mV/μm, and the EV structure radius $R_0 = 0.5 l_{\rm so}$ in Figs. 3 and 4.

The effectiveness of our self-consistent procedure is illustrated in Fig. 2. We plot the SC I_n^i (solid curves) at the system edge ($y = 0$) and at the EV boundary ($\rho = R_0$) in, respectively, Figs. 2(a) and 2(b). For comparison, we plot the SC source terms $f_i^{(1)}$ and $f_i^{(2)}$ (open symbols) in Figs. 2(a) and 2(b),

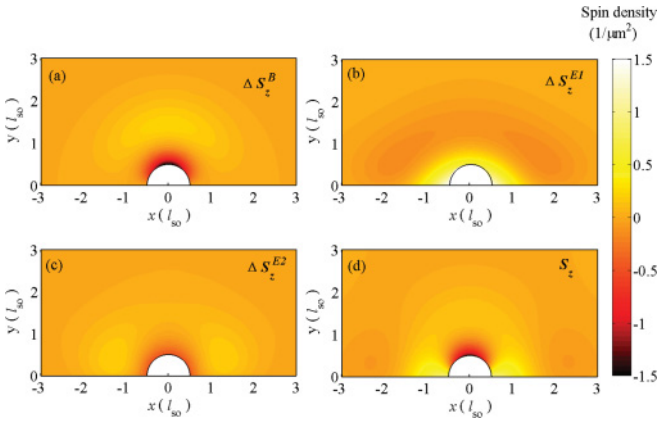

FIG. 3. (Color online) Out-of-plane spin densities ΔS_z^B, ΔS_z^{E1}, ΔS_z^{E2} and spin accumulation S_z are plotted in (a), (b), (c), and (d), respectively. Part (d) is the sum of (a), (b), and (c). The external electric field $\boldsymbol{E}$ is applied along $\hat{x}$ and the EV structure has a radius $R_0 = 0.5\, l_{\rm so}$.

respectively. Our result that all the six solid curves, three each for I_y^i and I_ρ^i, overlap on the zero abscissas shows that the SC boundary conditions are satisfied remarkably. Furthermore, the symmetries of the SC source are consistent with those derived from $\boldsymbol{S}^B$, as has been discussed in the previous section for the case of $f_i^{(1)}$.

Our main results are presented in Figs. 3 and 4. The former is the out-of-plane spin polarization, while the latter is the connection between the edge-spin accumulation and the bulklike spin flow represented by $f_z^{(1)}$. The spatial distribution of out-of-plane spin densities $\Delta \boldsymbol{S}_z^B$, $\Delta \boldsymbol{S}_z^{E1}$, and $\Delta \boldsymbol{S}_z^{E2}$ are shown, respectively, in Figs. 3(a), 3(b), and 3(c). The spin accumulation $\boldsymbol{S}_z$, given by the sum of these three out-of-plane spin densities, is denoted by Fig. 3(d). It is clearly shown that RSOI's contribution to spin accumulation $\boldsymbol{S}_z$ can be turned on locally by an EV due to the nonuniform driving field. Basically, Figs. 3(a)–3(c) provide a pictorial way of viewing the formation of the spin accumulation. Figure 3(a) shows the spin density $\Delta \boldsymbol{S}_z^B$ that equals that for a bulk void.[34] The spin density is centered along the $\phi = \pi/2$ direction and is

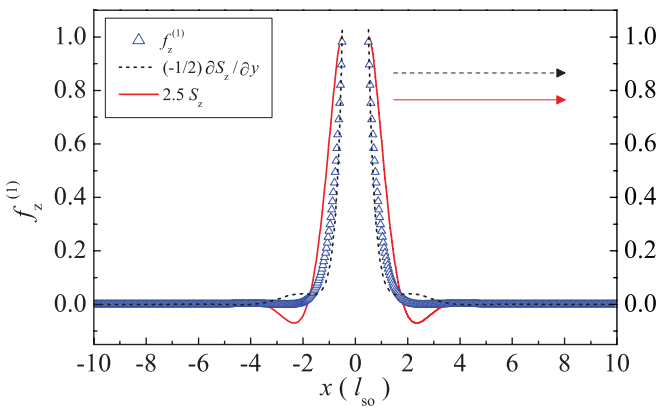

FIG. 4. (Color online) Spatial profiles of bulklike spin flow (SC source) $f_z^{(1)}$ (triangles), edge-spin accumulation S_z (solid line), and $-\partial S_z/\partial y$ (dashed line) at the sample edge ($y = 0$) for the edge void in Fig. 3. Numerical factors are introduced to facilitate comparison.

separated into two regions of opposite spin polarization: a core region and an outer region. The core region concentrates along the void boundary and has a radial thickness of about $0.3\, l_{\rm so} \sim 1.1\, \mu$m. The outer region has a much wider spatial extent, in the form of a curved spin cloud, and having its center located about a distance of one $l_{\rm so}$ from the void boundary. This spin density is driven by an in-plane SC of diffusive origin. The SC boundary condition is satisfied at the void boundary but not at the system edge. This results in a residual SC, or a SC source term $f_i^{(1)}$ [shown in Fig. 2(a)], at the system edge that drives the generation of $\Delta \boldsymbol{S}_z^{E1}$ in Fig. 3(b). The spin density $\Delta \boldsymbol{S}_z^{E1}$ concentrates mostly at the two corners of the EV with a range of about $0.5\, l_{\rm so}$ and with spin polarization opposite to that of the core spin density in Fig. 3(a). $\Delta \boldsymbol{S}_z^{E1}$ also contains a wide outer region of compensating spin cloud with much smaller spin-density magnitude. The SC boundary condition, however, is not satisfied at the void boundary. A residual SC, or a SC source term $f_i^{(2)}$, then drives the generation of the spin density $\Delta \boldsymbol{S}_z^{E2}$. Although the spin density $\Delta \boldsymbol{S}_z^{E2}$, in general, has a smaller magnitude, it enhances the core region in Fig. 3(a) at the void boundary. By our design, $\Delta \boldsymbol{S}_z^{E2}$ and $f_i^{(2)}$ together satisfy the SC boundary condition at both the system edge and the void boundary. This approach has the advantage that the self-consistently determined $\Delta \boldsymbol{S}_z^{E2}$ is of relatively small magnitude, thus, the method is numerically more stable and efficient. The total spin accumulation $\boldsymbol{S}_z$, as shown in Fig. 3(d), is the sum of the three spin densities.

Figure 4 compares the spatial profiles of the bulklike spin flow $f_z^{(1)}$ [also shown in Fig. 2(a)] and the total spin

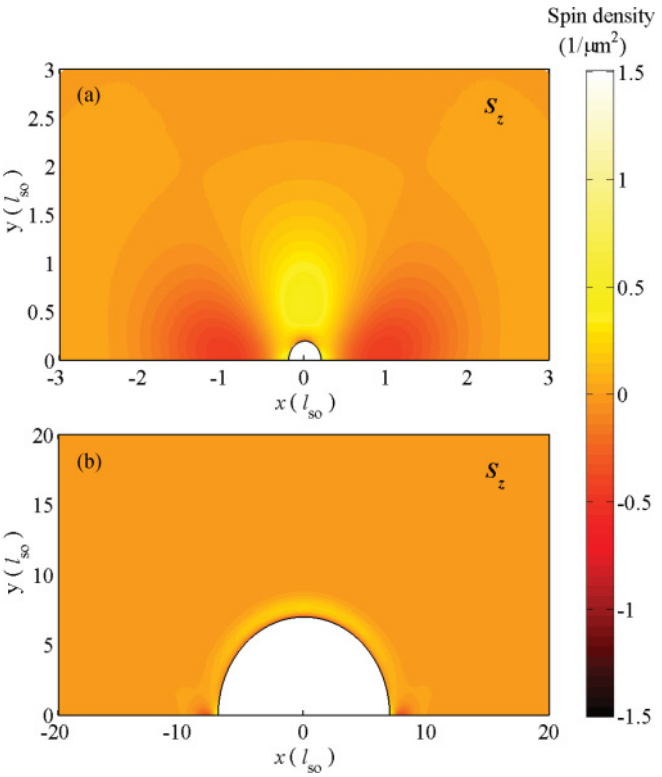

FIG. 5. (Color online) Total out-of-plane spin densities $\boldsymbol{S}_z$ for edge voids of radii $R_0 = 0.2\, l_{\rm so}$ and $R_0 = 7\, l_{\rm so}$ in (a) and (b), respectively.

accumulation S_z at the sample edge. Both characteristic behaviors of S_z, namely, S_z and $-\partial S_z/\partial y$, are included for the comparison, where $-\partial S_z/\partial y$ denotes the diffusive contribution of S_z to spin current. To facilitate the comparison, constant factors 2.5 and 0.5 are multiplied to S_z and $-\partial S_z/\partial y$, respectively. The spatial variation of $f_z^{(1)}$ in Fig. 4 matches very well with $-\partial S_z/\partial y$, except for the region $x \approx 2.5 l_{\rm so}$, where their values are already quite small. S_z also exhibits a similar spatial variation as $f_z^{(1)}$, except again at around $x \approx 2.5 l_{\rm so}$, when their respective values are small. The deviation comes from ΔS_y^{E1}, and the fact that it can contribute to I_y^z is seen in Eq. (7). We stress here that this close spatial correspondence between the bulklike spin flow and the characteristic behaviors of S_z in Fig. 4 collaborate the spin-current-driven nature of the edge-spin accumulation S_z. It also sheds light on spin injection, suggesting that the bulklike spin flow will be a driving agent for spin injection. We note that $f_z^{(1)}$ is chosen to represent the bulklike spin flow in the above consideration. The reason is that, in Fig. 2(a), $f_y^{(1)}$ is zero and $f_x^{(1)}$ does not couple with S_z, according to Eq. (7).

The magnitude of the out-of-plane $\boldsymbol{S}_z$ of EV is found to decrease in both large ($R_0 \gg l_{\rm so}$) and small ($R_0 \ll l_{\rm so}$) void radii. These two regimes are shown in Fig. 5 as contour plots of $\boldsymbol{S}_z$, and in Fig. 6 as the plots of the $\boldsymbol{S}_z$'s spatial variations along two representing directions, namely, along x and y, in Figs. 6(a) and 6(b), respectively. Comparing with the intermediate-radius regime ($R_0 = 0.5 l_{\rm so}$ in Fig. 3), three spatial modification features are found in $\boldsymbol{S}_z$ in both the small-radius [$R_0 = 0.2 l_{\rm so}$ in Fig. 5(a)] and large-radius [$R_0 = 7 l_{\rm so}$ in Fig. 5(b)] regimes. That the magnitude of $\boldsymbol{S}_z$ at the EV boundaries drops drastically is clearly shown in Figs. 6(a) and 6(b). The sizes of $\boldsymbol{S}_z$ clouds at the EV corners, positive $\boldsymbol{S}_z$ in the small $x - R_0$ region in Fig. 6(a), shrink drastically from $\sim l_{\rm so}$ to ~ 0.2–$0.3\, l_{\rm so}$. Finally, the thickness of the $\boldsymbol{S}_z$ at the void boundary, negative $\boldsymbol{S}_z$ in the small $y - R_0$ region in Fig. 6(b), shrinks from $\sim 0.3\, l_{\rm so}$ to less than $0.1\, l_{\rm so}$. These modifications in $\boldsymbol{S}_z$ can be understood as diminishing the effects of the nonuniform driving field for the case of large void radius. In the small-radius regime, however, different physical origins are at work for the $\boldsymbol{S}_z$ modifications. Since the entire vicinity of the EV is within a $l_{\rm so}$, the SC source terms $f_i^{(j)}$ can exert their effects to the region and, thus, no longer concentrated at the corner regions. This is supported, in Fig. 5(a), by the shrinking of the positive $\boldsymbol{S}_z$ at the void corners and the appearance of a positive $\boldsymbol{S}_z$ cloud around the $\phi = \pi/2$ direction. This positive $\boldsymbol{S}_z$ cloud has on its two sides negative $\boldsymbol{S}_z$ clouds, which are understood as the compensating spin cloud. Finally, this spin cloud configuration in Fig. 5(a) is expected to vanish as R_0 approaches zero. The integration of the SC source terms $f_i^{(j)}$ over the system edge (not shown) decreases to zero as $R_0 \to 0$.

The spin accumulation S_z can be probed optically by Kerr rotation. We plot, in Figs. 7(a) and 7(b), the net number of out-of-plane spin within a circular probe as it is scanned, respectively, along the directions $\phi = \pi/2$ and 0. The radius of the probe is the same as the void, and the distance between the probe and the void centers is d. For $\phi = \pi/2$, the net spin number exhibits a negative dip at small-d region and a large positive peak in the larger-d region. The former dip, located at around $d \approx 0.5\, l_{\rm so}$, picks up the core region, and the latter peak, located at around $d \approx R_0 + l_{\rm so}$, picks up the outer region of the spin accumulation. The system edge has only a mild effect on this curve, as is evident from the close resemblance of this curve to that of a bulk void. In contrast, for the $\phi = 0$ case, the

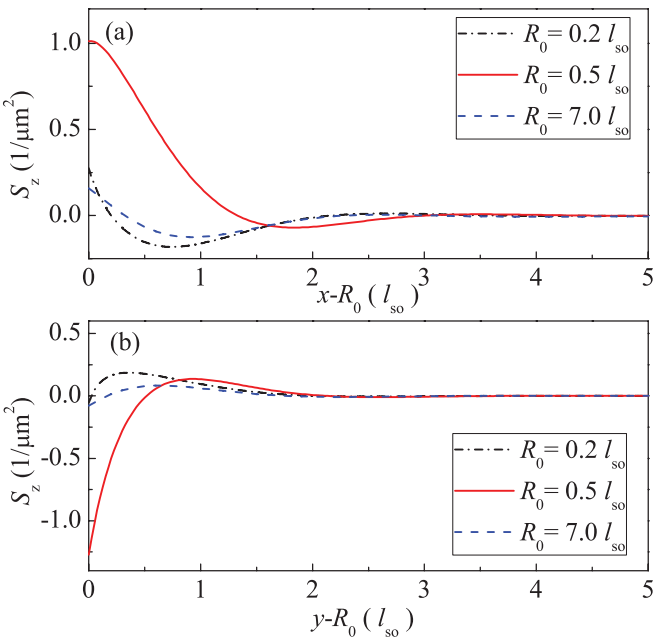

FIG. 6. (Color online) Spatial distribution of the total out-of-plane spin densities $\boldsymbol{S}_z$ for edge voids in Figs. 3 and 4 along (a) the x axis and (b) the y axis. The abscissas are the distances from the void edge.

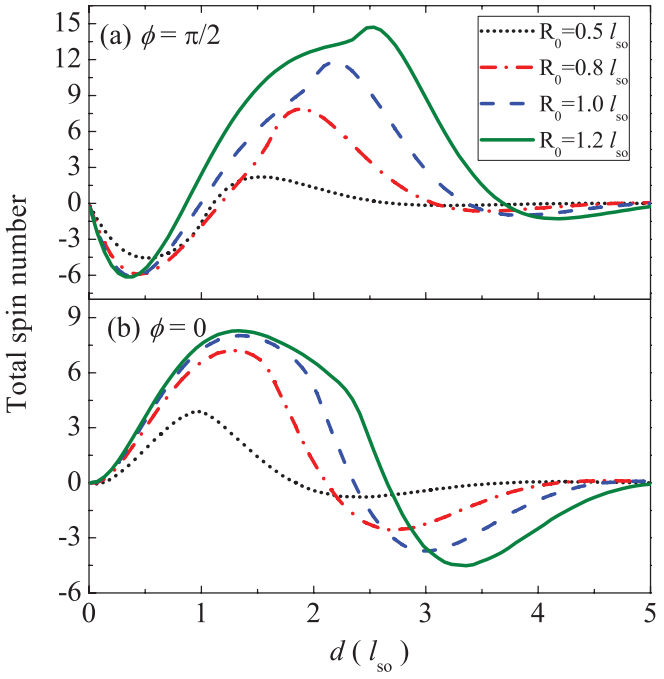

FIG. 7. (Color online) Net number of out-of-plane electron spins, from $\boldsymbol{S}_z$, within a circular probe area of the same radius as the EV structure. The probe center is shifted by a distance d from the EV center (a) along $\hat{y}$ ($\phi = \pi/2$) and (b) along edge ($\hat{x}$, or $\phi = 0$).

positive peak in the small-d region and the negative dip in the larger-d region reflects the sole effect of the system edge. The former peak, located at around $d \approx l_{so} - 1.3\,l_{so}$, picks up the spin accumulation at the corners of the EV, while the latter dip, located at around $d \approx 2R_0 + 0.8\,l_{so}$, corresponds to the situation when the probe moves out of the core region.

IV. CONCLUSIONS

In conclusion, we have studied in detail the physical processes of the formation of spin accumulation near an edge void and have demonstrated their spin-flow-driven nature. The EV structure reveals an underlying asymmetry of the bulk void, a nonzero bulklike spin flow on the $y = 0$ axis. The spin accumulation consists of both bulklike (void-boundary) and edgelike (system-edge) characteristics. Even though the edgelike spin accumulation has comparable magnitude but opposite signs compared with the bulklike spin accumulation, the two spin accumulations occur in different spatial locations so that the spin accumulation exhibits both characteristics simultaneously. Moreover, the spin accumulation and the bulklike spin flow correspond quite well in their spatial profiles at the system edge. This bulklike spin flow is expected to remain a driving agent for spin injection when a local protrusion occurs at the system edge. The EV structure could thus provide favorable sites for spin injection. These results should be of interest to further research in all-electric spintronics, both experimentally and theoretically.

ACKNOWLEDGMENTS

This work was supported by Taiwan NSC (Contract Nos. 96-2112-M-009-0038-MY3 and 100-2112-M-009-019), NCTS Taiwan, and a MOE-ATU grant.

[1] E. I. Rashba, Fiz. Tverd. Tela (Leningrad) **2**, 1224 (1960) [Sov. Phys. Solid State **2**, 1109 (1960)]; Yu. A. Bychkov and E. I. Rashba, Pis'ma Zh. Eksp. Teor. Fiz. **39**, 66 (1984) [JEPT Lett. **39**, 78 (1984)].
[2] J. Nitta, T. Akazaki, H. Takayanagi, and T. Enoki, Phys. Rev. Lett. **78**, 1335 (1997).
[3] D. Grundler, Phys. Rev. Lett. **84**, 6074 (2000).
[4] T. Bergsten, T. Kobayashi, Y. Sekine, and J. Nitta, Phys. Rev. Lett. **97**, 196803 (2006).
[5] J. I. Inoue, G. E. W. Bauer, and L. W. Molenkamp, Phys. Rev. B **70**, 041303(R) (2004).
[6] A. A. Burkov, A. S. Núñez, and A. H. MacDonald, Phys. Rev. B **70**, 155308 (2004).
[7] E. G. Mishchenko, A. V. Shytov, and B. I. Halperin, Phys. Rev. Lett. **93**, 226602 (2004).
[8] R. Raimondi and P. Schwab, Phys. Rev. B **71**, 033311 (2005).
[9] O. V. Dimitrova, Phys. Rev. B **71**, 245327 (2005).
[10] M. I. Dyakonov and V. I. Perel, Phys. Lett. A **35**, 459 (1971).
[11] A. A. Bakun, B. P. Zakharchenya, A. A. Rogachev, M. N. Tkachuk, and V. G. Fleisher, Pis'ma Zh. Eksp. Teor. Fiz. **40**, 464 (1984) [JETP Lett. **40**, 1293 (1984)].
[12] V. M. Edelstein, Solid State Commun. **73**, 233 (1990).
[13] A. G. Aronov, Yu. B. Lyanda-Geller, and G. E. Pikus, Zh. Eksp. Teor. Fiz. **100**, 973 (1991) [Sov. Phys. JETP **73**, 537 (1991)].
[14] J. E. Hirsch, Phys. Rev. Lett. **83**, 1834 (1999).
[15] S. Zhang, Phys. Rev. Lett. **85**, 393 (2000).
[16] S. Murakami, N. Nagaosa, and S. C. Zhang, Science **301**, 1348 (2003).
[17] J. Sinova, D. Culcer, Q. Niu, N. A. Sinitsyn, T. Jungwirth, and A. H. MacDonald, Phys. Rev. Lett. **92**, 126603 (2004).
[18] Y. K. Kato, R. C. Myers, A. C. Gossard, and D. D. Awschalom, Science **306**, 1910 (2004).
[19] S. Q. Shen, Phys. Rev. B **70**, 081311(R) (2004).
[20] J. Wunderlich, B. Kaestner, J. Sinova, and T. Jungwirth, Phys. Rev. Lett. **94**, 047204 (2005).
[21] A. G. Mal'shukov and K. A. Chao, Phys. Rev. B **71**, 121308(R) (2005).
[22] A. G. Mal'shukov, L. Y. Wang, C. S. Chu, and K. A. Chao, Phys. Rev. Lett. **95**, 146601 (2005).
[23] H. A. Engel, B. I. Halperin, and E. I. Rashba, Phys. Rev. Lett. **95**, 166605 (2005).
[24] W. K. Tse and S. Das Sarma, Phys. Rev. Lett. **96**, 056601 (2006).
[25] D. Culcer and R. Winkler, Phys. Rev. Lett. **99**, 226601 (2007).
[26] H. Saarikoski and G. E. W. Bauer, Phys. Rev. Lett. **102**, 097204 (2009).
[27] M. Duckheim, D. Loss, M. Scheid, K. Richter, I. Adagideli, and P. Jacquod, Phys. Rev. B **81**, 085303 (2010).
[28] B. K. Nikolić, S. Souma, L. P. Zârbo, and J. Sinova, Phys. Rev. Lett. **95**, 046601 (2005).
[29] J. Li and S. Q. Shen, Phys. Rev. B **76**, 153302 (2007).
[30] I. Adagideli and G. E. W. Bauer, Phys. Rev. Lett. **95**, 256602 (2005).
[31] A. Brataas, A. G. Mal'shukov, and Y. Tserkovnyak, New J. Phys. **9**, 345 (2007).
[32] R. Raimondi, C. Gorini, P. Schwab, and M. Dzierzawa, Phys. Rev. B **74**, 035340 (2006).
[33] R. S. Chang, C. S. Chu, and A. G. Mal'shukov, Phys. Rev. B **79**, 195314 (2009).
[34] L. Y. Wang, C. S. Chu, and A. G. Mal'shukov, Phys. Rev. B **81**, 115312 (2010).
[35] I. Adagideli, M. Scheid, M. Wimmer, G. E. W. Bauer, and K. Richter, New J. Phys. **9**, 382 (2007).
[36] The expressions for spin-current and spin-diffusion equations were shown (Ref. 34) to be valid for the nonuniform case.
[37] O. Bleibaum, Phys. Rev. B **74**, 113309 (2006).
[38] Y. Tserkovnyak, B. I. Halperin, A. A. Kovalev, and A. Brataas, Phys. Rev. B **76**, 085319 (2007).
[39] J. R. Shi, P. Zhang, D. Xiao, and Q. Niu, Phys. Rev. Lett. **96**, 076604 (2006).
[40] P. Zhang, Z. G. Wang, J. R. Shi, D. Xiao, and Q. Niu, Phys. Rev. B **77**, 075304 (2008).
[41] M. I. D'yakonov and V. I. Perel', Fiz. Tverd. Tela **13**, 3581 (1971) [Sov. Phys. Solid State **13**, 3023 (1972)].
[42] L. Meier, G. Salis, I. Shorubalko, E. Gini, S. Schön, and K. Ensslin, Nat. Phys. **3**, 650 (2007).